Microsystem Technologies (2020) 26:751–763
https://doi.org/10.1007/s00542-019-04629-3

TECHNICAL PAPER

Dielectrophoresis-based microfluidic platform to sort micro-particles in continuous flow

Mohsen Hajari[1,2] · Amirali Ebadi[1,2] · Mohammad Javad Farshchi Heydari[1,2,3] · Morteza Fathipour[1,2] · Madjid Soltani[3,4]

Received: 9 May 2019 / Accepted: 10 September 2019 / Published online: 17 October 2019
© Springer-Verlag GmbH Germany, part of Springer Nature 2019

Abstract

Non-invasive separation of particles with different sizes and sensitivities has been a challenge and interest for point-of-care diagnostics and personalized treatment. Dielectrophoresis is widely known as a powerful technique to sort the particles and (most importantly to) distinguish cells and monitor their state without the need for biochemical tags. In this paper, a dielectrophoresis-based microchannel design is proposed which allows for continuous particle sorting and separation under the applied AC field. It is also practical to implement the platform for monitoring cell behavior irregularities caused by certain diseases toward diagnosis and treatment. In this regard, the device employs dielectrophoretic (DEP) force exerted on the particles by only two electrodes with oblique arrangement in the channel. The electrodes are arranged with a bevel angle to the fluid flow direction but they are not parallel and therefore a gradually decreasing electric field is achieved along the channel's width. As a result, the dielectrophoretic force, acting on the particles of different sizes, would also gradually decrease along channels width which renders the necessary distinguishing lateral displacements of particles for separation. Therefore, the particles with different sizes can be sorted in a continuous-flow regime and be received at multiple outlet reservoirs with no need to turn the electric field on/off. The presented device is fabricated and evaluated in the experiment to prove its feasibility. Afterward, using numerical simulations, we investigate the optimum design parameters in the presented device to enhance device efficiency for separating particles with different size ranges.

1 Introduction

Harvesting particles and/or cells and their biological analysis plays an important role in various areas that include, but are not limited to, water and food quality (Andersson and Van den Berg 2003), environmental issues (Dockery et al. 1992), personalized diagnosis and treatment (Yang et al. 1999; Jackson and Lu 2013), and chemical and biomedical researches (Sackmann et al. 2014; Henkel et al. 2004; Guo et al. 2012; Joensson and Svahn 2012). Numerous methods and paradigms are proposed for cell manipulation and separation such as flow cytometry (Shapiro 2005), filtration (Yoon 2003), and cell isolation based on fluorescence (Fu et al. 1999). The necessity of cell sorting has recently expanded towards less populated cells like circulating fetal cells (CFCs), hematopoietic stem cells (HSCs) and circulating tumor cells (CTCs) from the blood (Armstrong et al. 2011; Wognum et al. 2003; Bischoff et al. 2003; Chen et al. 2014). Besides, the uprising movement toward personalized medicine would increase

Electronic supplementary material The online version of this article (https://doi.org/10.1007/s00542-019-04629-3) contains supplementary material, which is available to authorized users.

✉ Morteza Fathipour
mfathi@ut.ac.ir

[1] MEMS&NEMS Laboratory, Department of Electrical and Computer Engineering, Faculty of Engineering, University of Tehran, Tehran, Iran

[2] Device Simulation and Modeling Laboratory, Department of Electrical and Computer Engineering, Faculty of Engineering, University of Tehran, Tehran, Iran

[3] Department of Mechanical Engineering, K. N. Toosi, University of Technology, Tehran, Iran

[4] Centre for Biotechnology and Bioengineering (CBB), University of Waterloo, Waterloo, ON, Canada

the need for efficient separating devices more than before (Song et al. 2008). To accomplish this goal, many platforms are presented to meet the required accuracy and sensitivity for the aforementioned applications. Among different approaches, however, microfluidics has shown a promising precision and controllability in the detection and separation of particles in micro-scale (Zhang et al. 2016; Kamali et al. 2018). Furthermore, this technique enables high-throughput monitoring while using a small amount of rare or expensive samples in experiments (Forbes and Forry 2012). Such capabilities have encouraged many researchers to employ this technique to design and implement separation devices with considerable ease, accuracy, and functionality.

Microfluidic separation devices are categorized into active and passive types (Zhang et al. 2016). Passive separation devices mostly rely on design and geometry of the microchannel which sorts the particles on the basis of size, shape, and deformability (Zhang et al. 2016; Ebadi et al. 2019a, b); whereas, active types rely on external force fields acting on the flowing particles. Some widely used active types include acoustophoresis (AP) (Wang and Zhe 2011; Liu et al. 2019), magnetophoresis (MP) (Forbes and Forry 2012) and dielectrophoresis (DEP) (Çetin and Li 2011; Wu et al. 2017; Jung et al. 2017). Among these techniques, the dielectrophoresis provides controllable, accurate, and label-free cell separation and manipulation of targeted particles by inducing positive and negative effects on the samples and therefore is known as the most effective method (Çetin and Li 2011; Voldman 2006; Zhao K 2019). In the DEP method, the direction and magnitude of the exerted dielectrophoretic forces depends on the dielectric property of the sample (Pysher and Hayes 2007; Zhao et al. 2017) which corresponds to its chemical characteristics, morphology, and structure (Hughes 2002). This characteristic of the DEP enables a selective and sensitive analysis of bioparticles (Gascoyne et al. 2004).

Dielectrophoresis (DEP) is a non-destructive method for separating polarizable cells and bioparticles in a non-uniform electric field (Wu et al. 2017; Pethig 2010). The DEP platforms, traditionally, utilize microelectrodes embedded into the microfluidic chip to induce the non-uniform electric field (Pethig 2010; Zhang et al. 2010; Zhao and Li 2018). The particles with higher polarizability than their surrounding medium would experience positive DEP (p-DEP) and traverse towards areas with the most electric filed. Whereas, particles with lower polarizability (compared to suspending solution) undergo negative DEP (n-DEP) force and move toward lower electric fields (Zhao K 2019). As in the flowing carrier fluid, particles also experience the drag force. Wherever the dielectrophoretic force overpowers the hydrodynamic drag force, target particles are trapped and after the rest of the particles flown out of the microchannel, then the target particles would be released and received at the outlet reservoirs (Prieto 2010). Both of pDEP and nDEP forces are widely used to distinguish target particles or cells by sorting or trapping them from the carrier fluids. For instance, the blood components (Becker et al. 1994; Sano et al. 2011; Maria et al. 2017), stem cells (Song et al. 2015), cancer cells (Ghadami et al. 2017) can be mentioned. In order to improve DEP functionality and extend the active regions, various configurations, dimensions, and materials are proposed for the electrodes namely electroplated gold (Voldman et al. 2002), the liquid metal electrode (Sun et al. 2016; So and Dickey 2011; Tang et al. 2015), and AgPDMS (Lewpiriyawong et al. 2010, 2011).

Past researches mainly focused on batch-mode DEP separation of particles (i.e. trapping and release) which required precise control of valves and electric field, but there have been several efforts to separate cells and bioparticles in a continuous manner. Doh et al. (2005) devised a microfluidic platform employing dielectrophoresis and hydrodynamic forces to continuously separate viable and non-viable yeast cells that were successfully implemented with high purity. In another attempt, Kralj et al. (2006) developed a microfluidic platform and employed more than 300 bevel electrodes with a 45° angle with the flow and parallel to one another. They applied 10 V to electrodes with a frequency of 1 MHz. Under these circumstances, larger particles (6 μm polystyrene beads) were subjected to nDEP force moving them along width. Whereas smaller particles (4 μm polystyrene beads) experienced smaller nDEP forces and their trajectory was similar to flow direction and in this way, two different sizes of particles were separated. Collins et al. (2014) presented a similar method which they termed as virtual deterministic lateral displacement (vDLD). The method consisted interdigital transducers in a microfluidics chamber and produced the force field at an angle to separate particles over and below a critical size. In another attempt, Song et al. (2015) also established a similar design and by turning the electric field on/off repetitively so that particles (stem cells) experiencing stronger DEP would move along channel's width in several periods and particles (hMSCs) experiencing lower DEP force would remain on a straight trajectory. However, the active area of separation in these platforms consists most of the channel which would be a drawback when separating sensitive particles. Moreover, when in operation, these devices can only separate particles over and below a critical size; and for other sizes, the influencing parameters must change beforehand the operation which lacks tunability.

In this paper, a DEP design is proposed to continuously sort and separate cells and particles with employing AC electric field. The electrodes, similar to past researches, are

obliquely arranged to the fluid flow direction. We refrained from using parallel electrodes as it would result in a constant DEP force in the channel. We have innovated the presented geometry to achieve gradually decreasing nDEP force along the microchannel's width that allows for separating particles with variety of sizes (more than two) at outlet reservoirs and makes it unnecessary to turn the electric field on/off to cause the required lateral displacement for separation. The geometry includes only two electrodes that brings about reduced active area of the separating device which makes it suitable for sensitive particles sorting. Regarding each particle's properties, the particles of different sizes slide over the first electrode with distinguishing lateral displacements. Where the particles reach to the point that the exerted hydrodynamic force overpowers the dielectrophoretic force (release point), the lateral movement comes to an end and the particles follow the flow direction. Thereby, several groups of particles (of the same size) would be separated and received at the considered reservoirs. The proposing design is evaluated in experiment and the design's parameters are optimized for the best efficiency numerically. The excellent agreement between simulation and experiment verifies the validity of the proposed methodology.

2 Principle and design

When a non-uniform field is applied, polarizable particles form dipoles and experience a net force which results in their displacement. This motion is referred to as dielectrophoresis (Khoshmanesh et al. 2011) and exerted force is dielectrophoretic force which is a function of particle's shape and size, the ratio of dielectric properties of particle and medium, and the frequency and strength of applied electric field (Podoynitsyn et al. 2019). The dielectrophoretic force is expressed below (Jones and Jones 2005):

$$F_{DEP} = 2\pi R^3 \varepsilon_m \mathrm{Re}(f_{CM}) \nabla \left|E^2\right| \tag{1}$$

where R is particle's radius, ε_m is the electrical permittivity coefficient of the surrounding medium, $\nabla\left|E^2\right|$ is the local electric field gradient, and $\mathrm{Re}(f_{CM})$ is the real part of the Clausius–Mossotti coefficient which expresses a relation of complex permittivity of surrounding medium ($\overline{\varepsilon_m}$) and particle ($\overline{\varepsilon_p}$). For spherical particles, the Clausius–Mossotti coefficient is expressed as (Morgan and Green 2003)

$$f_{CM} = \left[\frac{\overline{\varepsilon_p} - \overline{\varepsilon_m}}{\overline{\varepsilon_p} + 2\overline{\varepsilon_p}}\right] \tag{2}$$

Complex permittivity ($\overline{\varepsilon}$)depends on angular velocity of applied electric field (ω) as well as the conductivity of the particle/cell (σ), where ε is permittivity and $j = \sqrt{-1}$ (Morgan and Green 2003).

$$\overline{\varepsilon} = \varepsilon - j\frac{\sigma}{w} \tag{3}$$

The sign of f_{CM} determines the direction of dielectrophoretic force and particle movement. For negative values, the particle would move toward regions with weaker electric fields which is negative DEP (nDEP). On the other hand, if the magnitude of f_{CM} is positive, the particle would traverse to regions with higher electric fields that is positive DEP (pDEP) (Gascoyne and Vykoukal 2004). As aforementioned, when electrodes are not parallel and are placed unorthodox to flow (see Fig. 1), the electric field gradient would not be constant between them and varies along the electrodes. This method can be utilized to continuously sort polarized particles like cells and polystyrene beads. Approaching toward the electrodes, particles first experience a weak nDEP force at first electrode's edge and therefore move toward its top. At the first electrode's end, strong electric field gradient acts on particles. Under these conditions, hydrodynamic drag and dielectrophoretic forces are exerted on particles. Figure 3 depicts electrodes schematic and acting forces on cells and particles. Also, it shows two important parameters of separation in this design (θ_1, θ_2) are electrodes' deviation from flow direction and when parallel, respectively. From now on, θ_1 and θ_2 will be referred to as "bevel" and "deviation" angles, respectively.

The dielectrophoretic (DEP) force is a result of the electric field gradient and is perpendicular to electrodes. The DEP force can be divided into its components in x- and y-direction. The $F_{DEP,x}$ is the dielectrophoretic force component in the x-direction which opposes the flow (before the electrodes) and the drag force direction. On the other hand, the $F_{DEP,y}$ would be perpendicular to the flow direction and forces particles to move downward in microchannel's width. The $F_{DEP,x}$ and $F_{DEP,y}$ are expressed below:

$$F_{DEP,x} = F_{DEP}\sin(\theta_1) \tag{4}$$

$$F_{DEP,y} = F_{DEP}\cos(\theta_1) \tag{5}$$

As particles approach the electrodes, DEP force increases so the particle's velocity declines till standstill. Afterward, vertical component of the DEP force ($F_{DEP,y}$) forces the particles to move downward along y-axis. As the electric field gradient decreases by an increasing distance between the two electrodes, the particle reaches a release point where the drag force overpowers the x-axis component of the DEP force. Thus, the release point position depends on several parameters such as the relative velocity of the fluid and particle (v), hydrodynamic viscosity of medium (η), the applied voltage on the electrodes (electric

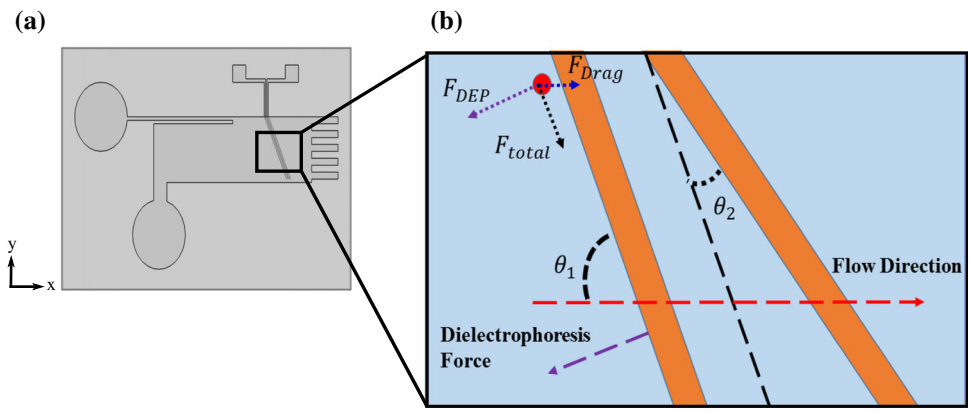

Fig. 1 Presenting electrode (brown) design and acting forces direction depiction. θ_1 is the angle between the first electrode and flow direction. Moreover, θ_2 is the difference between two electrodes in degrees. The DEP force is perpendicular to metal electrodes. Consequently, resultant force (F_{tot}) would be along the electrode and move the particles in this direction

field gradient), θ_1, θ_2, particles' size, dielectric properties of the medium and particle. Adjusting these parameters influence the efficiency and sensitivity of the presented device. Moreover, the electric field gradient is critically important at the release point for the separation of specific individual particles/cells. The gradient of the squared electric field at the release point is obtained below:

$$F_{Drag} = 6\pi\eta R v \tag{6}$$

$$F_{DEP,x} = F_{Drag} \tag{7}$$

From (1), (4), and (6):

$$2\pi R^3 \varepsilon_0 \varepsilon_m \mathrm{Re}(f_{CM}) \nabla \left|E^2\right| \cos\theta_1 = 6\pi\eta R v \tag{8}$$

Form (8), we would have (9) for the electric field gradient

$$\nabla \left|E^2\right| = \frac{3\eta v}{R^2 \varepsilon_0 \varepsilon_m \mathrm{Re}(f_{CM}) \cos\theta_1} \tag{9}$$

Also, we can assume "k" as defined in (10) to have the magnitude of the electric field gradient at the release point in (11)

$$k = \frac{3\eta v}{\varepsilon_0 \varepsilon_m \mathrm{Re}(f_{CM}) \cos\theta_1} \tag{10}$$

$$\nabla \left|E^2\right|_{x,th} = \frac{k}{R^2} \tag{11}$$

The magnitude of the electric field gradient at the release point ($(\nabla|E|^2)_{x,th}$) to overcome the drag force is given for any particle in (9) and (11). Thus, the critical $(\nabla|E|^2)_{x,th}$ can be calculated for each particle and thereby, the particle's release point coordinate would be predicted. Particles would move along the electrodes, experiencing a decline in the electric field gradient till they reach their release point at which the drag force overcomes the DEP force ($F_{DEP,x}$) and particles would flow out of the microchannel. The lateral displacement of a particle (Δy) before releasing can be expressed as in (12), where, L_0 is the distance which particle slides on the electrode before being released at the release point:

$$\Delta y = L_0 \sin(\theta_1) \tag{12}$$

Investigating (1) and (6), it is established that the drag force is linearly related to the particle's diameter which is comparable to the DEP force that is proportional to the cubic diameter of particles. Consequently, the particles with small diameters would have smaller $(\nabla|E|^2)_{x,th}$ and will be released with small lateral displacements. On the other hand, the particles with large diameters would have relatively more displacement along y-axis until being released and the separation takes place. By designing outlets at appropriate places, particles can be continuously sorted. The proposing micro-device has a 1 mm width, 50 µm height and 5 mm length. It has two inlets with 100 and 800 µm width for sample (particles/cells) and buffers, respectively. The electrodes are 50 µm wide and have a varying distance from each other which has a minimum of 50 µm. Figure 2 depicts characteristics of the designed microchannel, accompanied with an illustration of predicted particle trajectory. The geometry can be utilized to sort and separate variety of particles and can be optimized by modifying bevel and deviation angles in order to sort specific particles and size ranges.

3 Materials and methods

3.1 Device fabrication

Soft lithography is one of the cheapest and fastest methods to fabricate microfluidic chips. Here we are going to briefly mention the fabrication process of the proposed microdevice. First, a thin layer of SU-8 2050 photoresist (MicroChem, Newton, MA, USA) with 50 µm thickness was spin-coated on a glass substrate and then UV light was used to produce the mold. Afterward, standard mixture of polydimethylsiloxane (PDMS, Sylgard 184, Dow Corning,

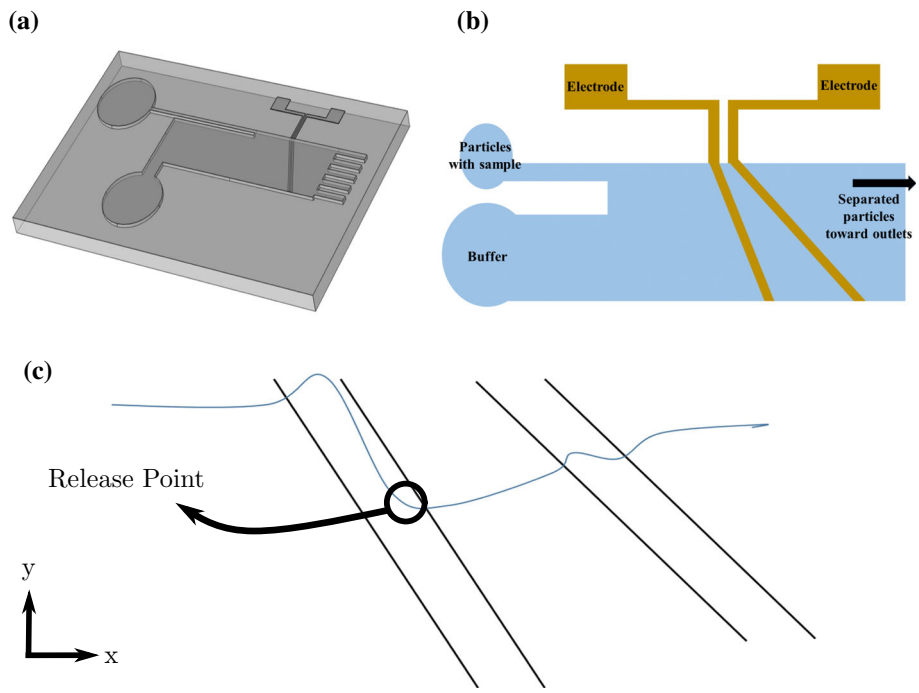

Fig. 2 **a** Depiction of the whole channel's structure. **b** Sample, buffer inlets and two electrodes are located as shown. **c** Bird's eye view of an illustration of predicted particle trajectory: When particles approach first electrode's left edge, it moves toward the micro-channels ceiling. At the right edge of the first electrode, the strong gradient of the electric field is applied on particles and force them to move along the electrode until they reach their release point

USA) and its curing was poured, heated, and peeled off which then contained our design. To fabricate the electrodes, at first, 40 nm chrome layer was coated on the substrate to play the adhesion layer role. Secondly, a 100 nm gold layer is blanketed by RF Sputter. Afterward, the electrodes' design was lithographed by AZ ECI 3000 photoresist (Micro-Chem, Newton, MA, USA). Finally, the chrome and gold layers were wet-etched to obtain the electrodes. Resulting electrodes and engraved channel design on the PDMS was bound by oxygen plasma. The fabricated microdevice is shown in the Fig. 3. The device is 50 µm and has two inlets with 100 µm and 800 µm which are considered for the particle mixture and buffer, respectively (see Fig. 2b). To collect the separated particles, three outlets are designed with 200 µm width. The metal electrodes in the microchannel's bottom are 50 µm wide and are placed with 50 µm distance from each other which increases along the channel's width.

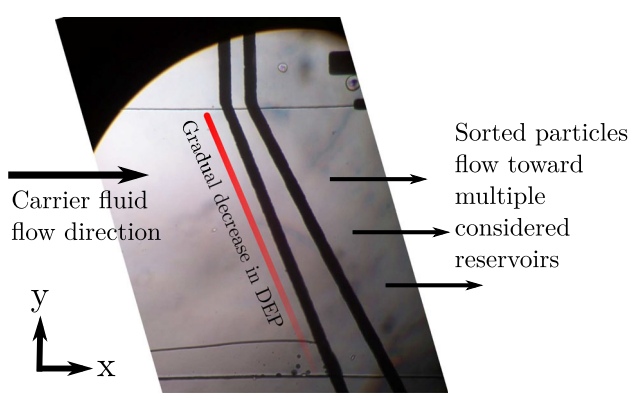

Fig. 3 Fabricated microchannel with embedded electrodes. The electrodes are made of chrome and gold. The particles with different sizes enter the microchannel as a part of the carrier fluid and are sorted after they pass the electrodes. The gradual decrease in DEP force along y-axis direction occurs as the distance between the interdigitated electrodes increase. As a result, the particles with larger diameters would have more lateral displacement that enables sorting with no need to turn the electric field on/off

3.2 Quantitative analysis

To evaluate the device's functionality, sorting particles and cells were numerically simulated by the finite element method (FEM). The fluid flow, particle trajectories, and the electric field gradient were considered to obtain realistic results. To investigate the device sensitivity and accuracy in respect to particles sizes, bioparticles and polystyrene beads were employed as the testing materials. In several steps, polystyrene beads with different size ranges and the blood cells were numerically sorted by the presented geometry. The achieved results are presented in the results section. The fluid flow profile with the particles was simulated with an initial velocity of 10^{-3} m/s. The polystyrenes particles are considered to have 2200 kg/m^3 density and no charge in simulation. Also, the Stokes drag law in addition to the dielectrophoresis force is considered with particle relative permittivity of 2.5 and electrical conductivity of 1.2e−3 S/m. Besides, the fluid relative permittivity is considered to be 78 and its electrical conductivity to be 2e−4 S/m. To simulate the electric field in the channel, AC electric field with voltage of 40 volts is

applied between the considered gold electrodes while the angular frequency of 60e6 rad/s affects all the particles.

The distribution of the electric field gradient in electrodes is of high importance. When the two electrodes are patterned at the bottom of the microchannel, a strong electric field gradient occurs between them and charges move to edges. Therefore, these electrodes can be modeled as four charged lines in the FEM to investigate how electric field gradient varies around edges in different heights. By the Fig. 4, it is established that, as expected, the maxima of the electric field gradient happen between the two electrodes and around their edges. The magnitude of electric field gradient gradually decreases from the bottom of the microchannel to its top but it's constant in electrodes length. Moreover, the magnitude of the electric field is a function of distance from the channel's bottom and electrode's distance from each other. In another illustration, in Fig. 5a, b one line and plane are plotted respectively at an arbitrary height of 49 µm to show electric field gradient between the two parallel electrodes. The sharp spikes in the Fig. 4c are related to the high gradients at the edges.

4 Results and discussion

Separating particles with a variety of sizes are controlled by several parameters in our presented geometry and channel's characteristics. Among them, some are critical and influencing like the angle of the first electrode and flow direction (Bevel angle or θ_1) and the difference of two

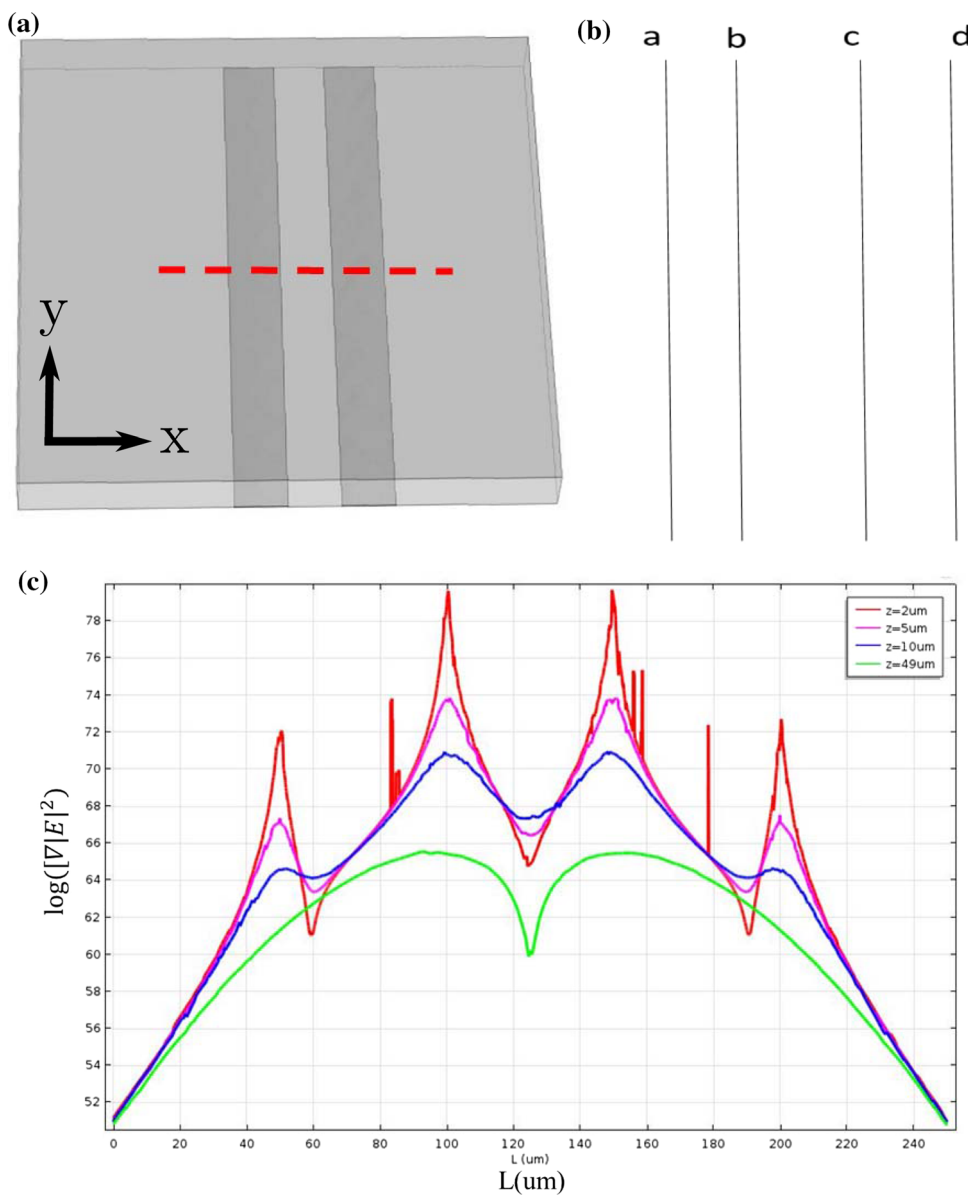

Fig. 4 **a** A sketch of $\log(\nabla|E|^2)$ along the width of a 250 µm wide microchannel with two metal electrodes at its bottom. **b** Microelectrodes resemble four charged lines as the electric charges appear on the edges. **c** The electric field gradient in the microchannel's width in several heights from its bottom. Simulation was carried out for the line heights 2 µm (red), 5 µm (pink), 10 µm (blue) and 49 µm (green) from channel's bottom

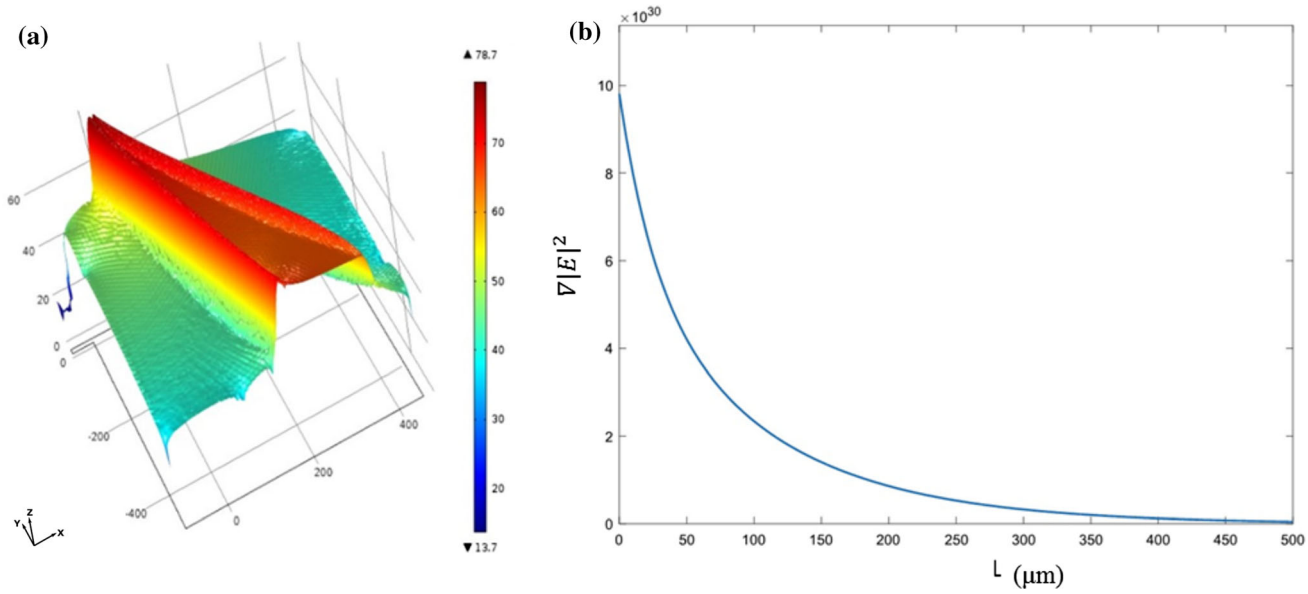

Fig. 5 Electric field gradient in micro-channel in **a** a plane at h = 49 μm from channel's bottom and **b** a cutline in h = 49 μm and left edge of the first electrode in the sketched arbitrary line

electrodes in degrees (deviation angle or θ_2) (see Fig. 1). In this section, the functionality of the separation platform and validation of the design is accomplished experimentally by introducing polystyrene beads to the channel. Then, the sensitivity and resolution of the device are optimized to separate particles with close range sizes (8, 9 and 10 μm) and wide range sizes (10, 20 and 30 μm) numerically.

4.1 Experimental setup

To evaluate the channel's functionality in the experiment, as mentioned in the simulation section, polystyrene beads are employed. The device was prepared to conduct an experiment by the following steps. At first, the channel was rinsed with Phosphate Buffered Saline (PBS) buffer. Secondly, electrodes were connected to an AC voltage with 10 Vp-p and 200 kHz by platinum wires. At last, inlets were connected to two micropumps to supply a constant velocity of 1 mm/s. When the voltage is applied, the particles would be trapped and have a lateral displacement along the electrodes until they reach their release point and flow out of the channel. Figure 6 is generated from overlapping consecutive frames achieved from experiment and simulation results over a 1.5 s span. Figure 6 illustrates a qualitative comparison of obtained particle trajectory by the simulation and experiment. It is established that the polystyrene bead enters the channel and then has a lateral displacement till it reaches to the point in which the hydraulic drag force and the dielectrophoresis forces become equal. Afterward, the polystyrene bead is released and moves toward its designed outlet. By the Fig. 6, it is evident that the experiment and simulation results are in excellent agreement which sets the stage for further simulation studies for the optimization of the device.

4.2 Bevel angle (θ_1) effect on separation

Separation efficiency can be influenced by a bevel angle of θ_1. Equation (4) expresses the horizontal component of the DEP force opposing drag force which is impacted by θ_1.

As the θ_1 converges to 90°, the DEP force becomes more intense in the x-direction. Thus, particles would have more lateral displacement to reach their release point which increases the device's sensitivity or in other words, the efficiency of separation regarding physical characteristics of particles increases. However, when θ_1 is 90° (left electrode and flow direction are perpendicular to each other), separation would not happen. Besides, the vertical component of the DEP force causing lateral displacement of particles would be zero and therefore particles cannot move in the y-direction. Whereas, if θ_1 converge to zero (left electrode and flow direction are parallel), the horizontal component of DEP would be negligible and more voltage should be applied to prevent straight transverse of particles. So, a reasonable harmony is critical to accomplish the optimal separation conditions. Figure 7 shows the effect of θ_1 on $F_{DEP,x}$ and $F_{DEP,y}$ and exhibits that increasing the θ_1 would result in the increase of the DEP force in the x-direction (Fig. 7a) and decrease in the y-direction (Fig. 7b).

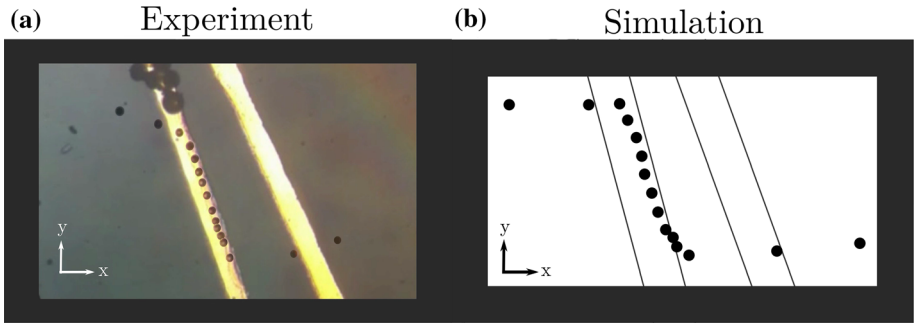

Fig. 6 Polystyrene particle trajectory in the device in **a** experiment and **b** simulation by finite element method. As the particle approaches the first electrode, it undergoes a lateral displacement due to the high electric field gradient. Then, when the particle reaches its release point, drag force overcomes the dielectric force and force the particle towards outlets. Both in simulation and experimental setup, the electrodes have AC voltage of 10 Vp-p and 200 kHz. This figure is generated from overlapping consecutive frames of achieved results. The video is available as online supplementary materials

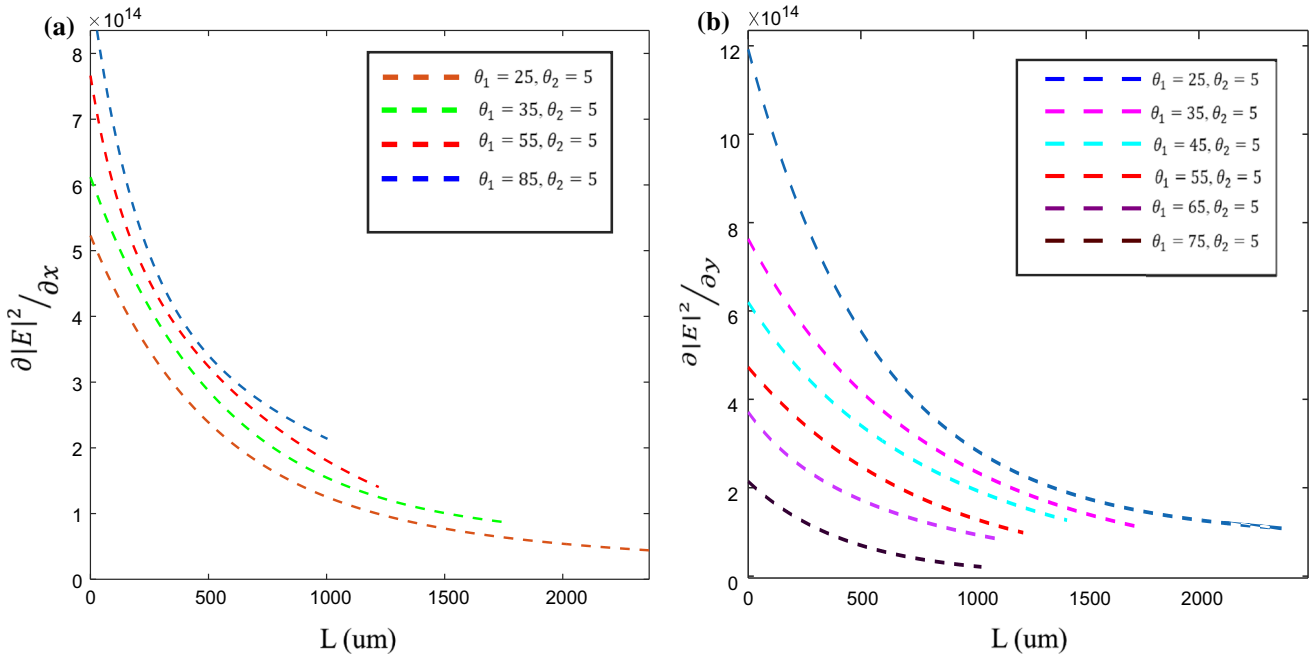

Fig. 7 The electric field gradient at the right edge of the first electrode and h = 49 µm, simulated by FEM. θ_2= 5° is constant. Increasing θ_1 causes **a** increase in the gradient of squared electric field magnitude along the flow direction (x-axis). **b** Decrease in the gradient of squared electric field magnitude proportional to flow direction (y-axis)

4.3 Deviation angle (θ_2) effect on separation

The gradual decrease of $(\nabla|E|^2)_x$ (as the distance between the two electrodes increases) can be controlled by the deviation angle (θ_2). Moreover, it can influence the separation resolution for specific applications. For instance, when the angle is zero (electrodes are parallel), $(\nabla|E|^2)_x$ would be constant and will not change in the microchannel's width. Therefore, the cells would pile up and trapped and will not be able to pass the electrodes. Increasing the θ_2, we can reduce $(\nabla|E|^2)_x$ between the two electrodes and particles would reach their release point with less lateral displacement. Thus, this structure enables us to modify the design for different fluids and/or particles. For instance, the sorting of particles with wide size differences (for instance particles with 10, 20, and 30 µm) would require less sensitivity and thereby, more θ_2 will be functional as well. Figure 8 shows a decline in the electric field gradient in respect to θ_2 increase.

4.4 Separation of 2, 5 and 8 µm polystyrene beads

Sorting polystyrene beads with 2, 5, and 8 µm requires geometry modification so that smallest bead would not be trapped and also the particles would have sufficient lateral

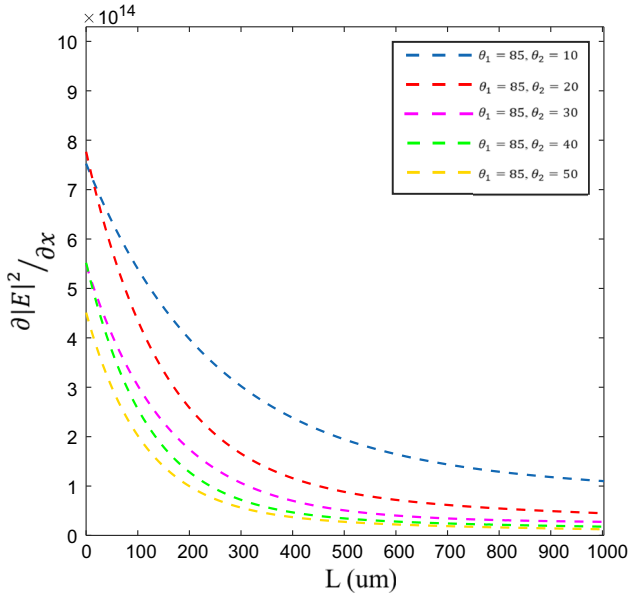

Fig. 8 The obtained magnitude of electric field gradient between electrodes while θ_2 is decreased. θ_1 was constant and equal to 85°

displacement for highest possible resolution in separation. However, the dielectrophoresis force should be enough to force particles to move along the first electrode to reach their release point. The critical magnitude of electric field gradient ($(\nabla|E|^2)_{x,th}$) is calculated for polystyrene beads with different sizes. Figure 9 shows the $(\nabla|E|^2)_x$ in the first electrode and at 49 µm from channel's bottom with different θ_2 angels. According to Fig. 9 and Eq. (12), the lateral displacement of each particle before releasing is calculated to make sure that particles have distinguishing values of Δy for separation. Two horizontal lines are drawn in Fig. 9a, b representing the critical magnitude of electric field gradient for 5 and 8 µm particles which are in fact, these particles' release point. It is established that the polystyrene beads would not be separated under $\theta_1 = 65$, $\theta_2 = 5$ and $\theta_1 = 85$, $\theta_2 = 5$ conditions since the separation of 8-µm particles requires reaching less magnitude of electric field gradient than reached by these configurations or in other words 8 µm particles would be trapped. It is noteworthy to mention that to find an optimum configuration to sort 5 and 8 µm polystyrene beads among remaining possible conditions, more lateral distance between the two particles before reaching their releasing point is desirable in outlets and will be achieved with $\theta_1 = 65$, $\theta_2 = 15$.

Figure 9c shows the particle trajectories of 2, 5, and 8 µm particles under most favorable configuration, simulated by the FEM. Two micrometers (2 µm) particles move almost straight out of the device. But, 5 and 8-µm particles experience a strong electric field gradient and are forced to have different amounts of lateral movements toward less electric field gradient until they reach their release point.

4.5 Separation of 8, 9 and 10 µm polystyrene beads

Under these circumstances, as the polystyrene beads are close in diameter (only 1 µm difference), the device's size sensitivity is critically important. Figure 10a is sketched for two θ_1 angles of 85° and 45° and the critical electric field gradient for 9- and 10-µm particles are drawn as horizontal lines so that optimum configuration would be easier to choose. Again, lateral displacement can be computed according to Fig. 10a and Eq. (12). Lateral displacement would be at its optimum for θ_1 =85°, θ_2 = 5° as the release point of 9 and 10 µm particles have the most lateral displacement.

4.6 Separation of 10, 20 and 30 µm polystyrene beads

Particles with wide size ranges do not require high sensitivity of design and fabrication. Figure 11 illustrates $(\nabla|E|^2)_x$ at the right edge of the first electrode at h = 49 µm. A horizontal line is drawn to show critical $(\nabla|E|^2)_{x,th}$ for 20 and 30 µm polystyrene beads. Once more, the lateral displacement of each particle is calculated utilizing Eq. (12) and Fig. 11. It is established by the Fig. 11 that the particles with 30 micrometers diameter cannot be separated with $\theta_1 = 85°$, $\theta_2 = 5°$ condition. Optimal lateral displacement is achieved under $\theta_1 = 85°$, $\theta_2 = 35°$ configurations. Figure 11b shows particle trajectories with the obtained most favorable conditions ($\theta_1 = 85°$, $\theta_2 = 35°$).

4.7 Blood cells separation

Unlike the polystyrene beads, the blood cells cannot be assumed as rigid spheres. Cells have different layers like cytoplasm and membrane that each has unique characteristics that must be considered for reliable numerical simulation of these cells and their separation processes. Required characteristics of blood cells for separation simulation are tabulated in Table 1.

For multilayer structures, like cells, a single shell model can be considered and the complex permittivity can be estimated using Eq. (13) to calculate the Clausius–Massoti coefficient (Shafiee et al. 2010):

$$\overline{\varepsilon_p} = \overline{\varepsilon_{mem}} \frac{\gamma^3 + 2\left(\frac{\overline{\varepsilon_i} - \overline{\varepsilon_{mem}}}{\overline{\varepsilon_i} + 2\overline{\varepsilon_{mem}}}\right)}{\gamma^3 - \left(\frac{\overline{\varepsilon_i} - \overline{\varepsilon_{mem}}}{\overline{\varepsilon_i} + 2\overline{\varepsilon_{mem}}}\right)} \tag{13}$$

where "i" and "mem" indices represent cytoplasm and membrane, respectively, $\gamma = \frac{r}{r-d}$, r is the particle radius,

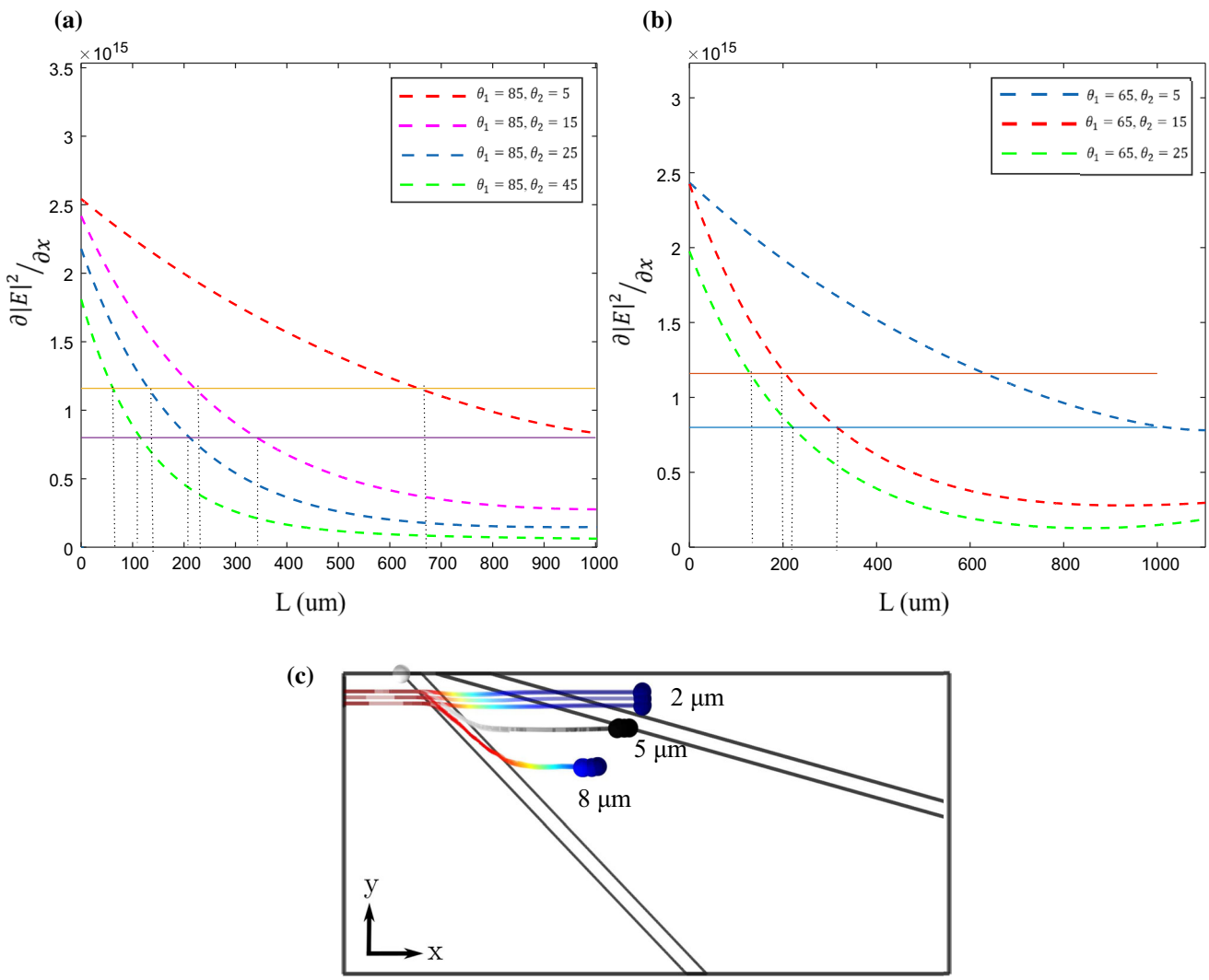

Fig. 9 Electric field gradient in the flow direction is depicted at the right edge of the first electrode and 49 µm high from bottom of the microchannel. Two horizontal lines are sketched to show critical $(\nabla|E|^2)_x$ for 5 and 8 µm particles. Obtained values of squared electric field gradient for a) θ_1 = 85° and θ_2= 5°, 15°, 25° and 45° along with **b** θ_1 = 65° and θ_2= 5°, 15° and 25° are drawn. **c** Particle trajectories of 2, 5, and 8 µm under θ_1 = 65, θ_2 = 15 are simulated by the FEM. The particles slide along the first (left) electrode to reach their release point and then flow out of the micro-device

and d is the membrane thickness (Morgan and Green 2003; Morgan et al. 2006).

Similar to previous numerical simulations, the separation of blood components was carried out under several angle configurations to find the optimum properties for the separation. Figure 12 depicts the electric field gradient under mentioned circumstances and the RBC and WBC critical $(\nabla|E|^2)_{x,th}$ is are exhibited by horizontal lines according to Table 1. Applying the Eq. (12), each particle's lateral displacement can be obtained. According to Fig. 12a, the white blood cells would not be separated under the configuration of θ_1 = 45°, θ_2 = 5° and the lateral displacement would be optimal with θ_1 =45°, θ_2 = 15° arrangement. Figure 12b illustrates the computed particle trajectory of RBC, WBC, and platelets with the optimal geometry.

5 Conclusion

In this paper, we presented a continuous-flow, dielectrophoresis-based microfluidic platform to sort and separate particles with different sizes and sensitivities. Using only two oblique electrodes, the device has a low active area which leaves the least effect on the sensitive target particles. In the proposing design, unlike previous studies, the two electrodes are non-parallel which brings about decreasing dielectrophoretic force in microchannel's width as the distance between the two electrodes increases. The

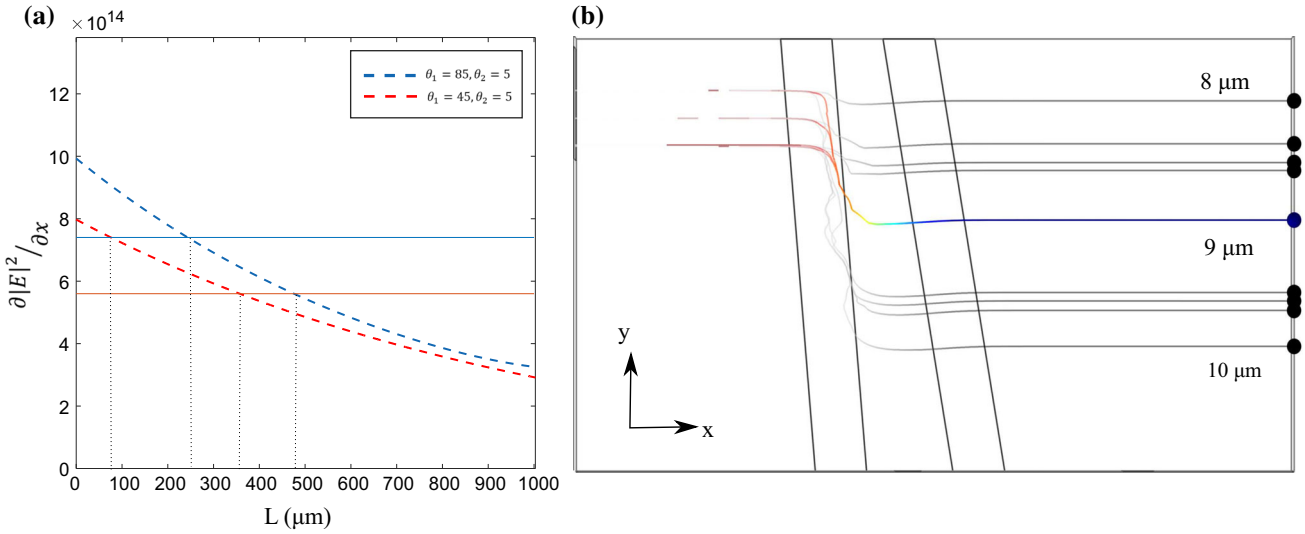

Fig. 10 **a** Depiction of obtained values for the electric field gradient in the flow direction at the right edge of the first electrode and h = 49 μm height for θ_1 = 85 and 45, θ_2 = 5. Two horizontal lines are sketched to show critical electric field gradient calculated for 9 and 10-μm particles. **b** Simulated particle trajectories assuming θ_1 = 85°, θ_2 = 5° for the 8, 9 and 10-μm beads

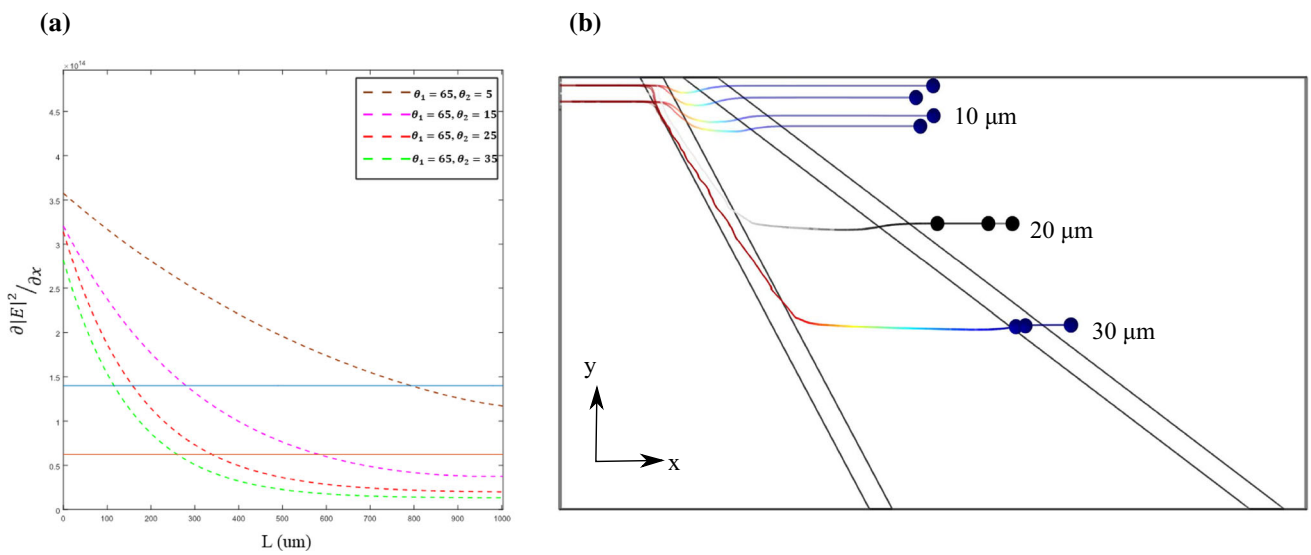

Fig. 11 **a** The electric field gradient at the right edge of the first electrode at h = 49 μm. Calculated for θ_1 = 85°, θ_2 = 5°, 15°, 25° and 35°. The two horizontal lines represent the square of the critical electric field gradient for the 20 and 30 μm particles. **b** Particle trajectory simulation of 10, 20 and 30 μm bead under the condition of θ_1 = 65°, θ_2 = 35°

Table 1 Platelet, RBC, and WBC characteristics such as electrical permittivity and conductivity of membrane and cytoplasm, diameter, and membrane thickness

Cell/ characteristic	Diameter (μm)	Cytoplasm electric conductivity (s/m)	Cytoplasm electric permittivity	Membrane electric conductivity (s/m)	Membrane electric permittivity	Membrane thickness (nm)
Platelet	1.8	0.255	50	1×10^{-4}	6	8
Red blood cell	5	0.315	59	1×10^{-4}	4.44	9
White blood cell	8	0.4	61	1×10^{-4}	3	10

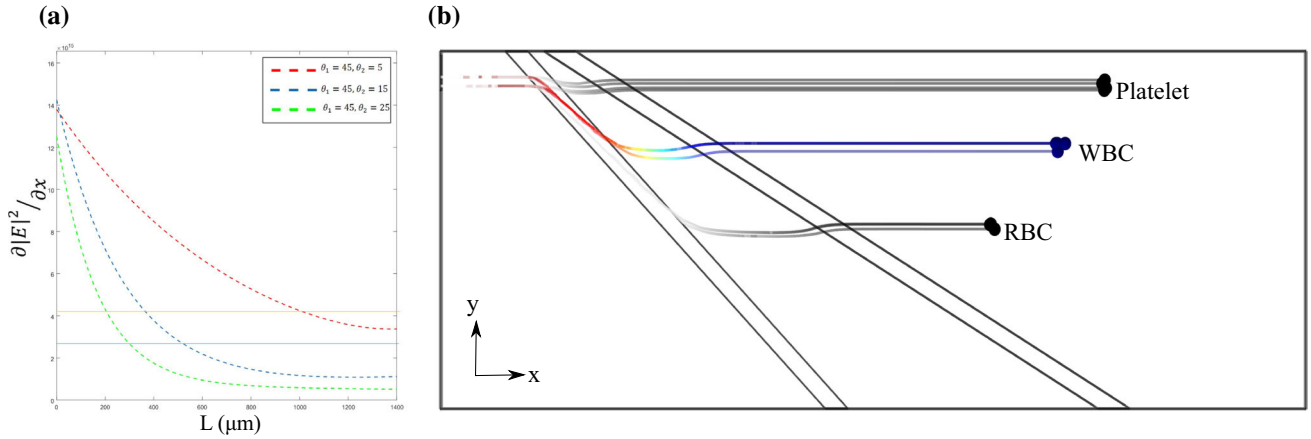

Fig. 12 **a** The electric field gradient at the right edge of the first electrode when the distance from the channel's bottom is h = 49 μm. Angle configuration is $\theta_1 = 45°$ and $\theta_2 = 5$, 15, 25. Two horizontal lines show critical electric field gradient, in the flow direction, for RBC and WBC release. Separation of blood cells by $\theta_1 = 45°$, $\theta_2 = 15°$ arrangement of electrodes. **b** Using $\theta_1 = 45°$, $\theta_2 = 15$ configurations, particle trajectories of the RBC, WBC, and platelets are simulated

electrodes are arranged oblique to the flow direction in order to cause the required lateral displacement for separation. Therefore, a variety of particles with different sizes can be sorted in operation and with no on/off electric field. Several numerical simulations are carried out to optimize significant design parameters for separation of particles with different size ranges. The simulation and experiment results of the proposed platform are in excellent agreement and support the feasibility of the microdevice. As an outlook for this promising platform, it should be noted that every cell in this device would have a specific release point, and thereby, particles and/or cells would also have unique trajectories. Thus, when a disease changes the properties of blood cells or an external cell enters the blood, a new trajectory and movement pattern will be observed. By knowing how each disease changes the cells' properties and cells' movement patterns, diseases would be diagnosed without the need of employing biomarkers which increase the experiment cost. The authors hope that the presented platform pave the way for fast diagnosis and treatment of illnesses as a part of point-of-care diagnosis technology.

References

Andersson H, Van den Berg AJS (2003) Microfluidic devices for cellomics: a review. Chemical 92(3):315–325

Armstrong AJ et al (2011) Circulating tumor cells from patients with advanced prostate and breast cancer display both epithelial and mesenchymal markers. Mol Cancer Res 9:1007

Becker F et al (1994) The removal of human leukaemia cells from blood using interdigitated microelectrodes. J Phys D Appl Phys 27(12):2659

Bischoff F et al (2003) Intact fetal cell isolation from maternal blood: improved isolation using a simple whole blood progenitor cell enrichment approach (RosetteSep^{TM}). Clin Genet 63(6):483–489

Çetin B, Li D (2011) Dielectrophoresis in microfluidics technology. Electrophoresis 32(18):2410–2427

Chen Y et al (2014) Rare cell isolation and analysis in microfluidics. Lab Chip 14(4):626–645

Collins DJ, Alan T, Neild AJLOAC (2014) Particle separation using virtual deterministic lateral displacement (vDLD). Lab on a Chip 14(9):1595–1603

Dockery DW, Schwartz J, Spengler JDJER (1992) Air pollution and daily mortality: associations with particulates and acid aerosols. Environ Res 59(2):362–373

Doh I, Cho YHJS, Physical AA (2005) A continuous cell separation chip using hydrodynamic dielectrophoresis (DEP) process. Sens Actuators A Phys 121(1):59–65

Ebadi A et al (2019a) Efficient paradigm to enhance particle separation in deterministic lateral displacement arrays. SN Appl Sci 1(10):1184

Ebadi A et al (2019b) A novel numerical modeling paradigm for bio particle tracing in non-inertial microfluidics devices. Microsyst Technol 2019:1–9

Forbes TP, Forry SP (2012) Microfluidic magnetophoretic separations of immunomagnetically labeled rare mammalian cells. Lab Chip 12(8):1471–1479

Fu AY et al (1999) A microfabricated fluorescence-activated cell sorter. Nature 17(11):1109

Gascoyne PR, Vykoukal JV (2004) Dielectrophoresis-based sample handling in general-purpose programmable diagnostic instruments. Proc IEEE 92(1):22–42

Gascoyne PR et al (2004) Dielectrophoresis-based programmable fluidic processors. Lab Chip 4(4):299–309

Ghadami S et al (2017) Spiral microchannel with stair-like cross section for size-based particle separation. Microfluid Nanofluid 21(7):115

Guo MT et al (2012) Droplet microfluidics for high-throughput biological assays. Lab Chip 12(12):2146–2155

Henkel T et al (2004) Chip modules for generation and manipulation of fluid segments for micro serial flow processes. Chem Eng 101(1–3):439–445

Hughes MP (2002) Strategies for dielectrophoretic separation in laboratory-on-a-chip systems. Electrophoresis 23(16):2569–2582

Jackson EL, Lu H (2013) Advances in microfluidic cell separation and manipulation. Curr Opin Chem Eng 2(4):398–404
Joensson HN, Svahn HAJACIE (2012) Droplet microfluidics—a tool for single-cell analysis. Angew Chem Int Ed 51(49):12176–12192
Jones TB, Jones TB (2005) Electromechanics of particles. Cambridge University Press, Cambridge
Jung Y-J et al (2017) Selective position of individual cells without lysis on a circular window array using dielectrophoresis in a microfluidic device. Microfluid Nanofluid 21(9):150
Kamali B et al (2018) Micro-lithography on paper, surface process modifications for biomedical performance enhancement. Colloids Surf A Physicochem Eng Aspects 555:389–396
Khoshmanesh K et al (2011) Dielectrophoretic platforms for bio-microfluidic systems. Biosens Bioelectron 26(5):1800–1814
Kralj JG et al (2006) Continuous dielectrophoretic size-based particle sorting. Anal Chem 78(14):5019–5025
Lewpiriyawong N, Yang C, Lam YC (2010) Continuous sorting and separation of microparticles by size using AC dielectrophoresis in a PDMS microfluidic device with 3-D conducting PDMS composite electrodes. Electrophoresis 31(15):2622–2631
Lewpiriyawong N et al (2011) Microfluidic characterization and continuous separation of cells and particles using conducting poly (dimethyl siloxane) electrode induced alternating current-dielectrophoresis. Anal Chem 83(24):9579–9585
Liu G et al (2019) Multi-level separation of particles using acoustic radiation force and hydraulic force in a microfluidic chip. Microfluid Nanofluid 23(2):23
Maria MS et al (2017) Capillary flow-driven blood plasma separation and on-chip analyte detection in microfluidic devices. Microfluid Nanofluid 21(4):72
Morgan H, Green NG (2003) AC electrokinetics. Research Studies Press, UK
Morgan H et al (2006) Single cell dielectric spectroscopy. J Phys D App Phys 40(1):61
Pethig R (2010) Dielectrophoresis: status of the theory, technology, and applications. Biomicrofluidics 4(2):022811
Podoynitsyn SN et al (2019) Barrier contactless dielectrophoresis: a new approach to particle separation. Sep Sci Plus 2(2):59–68
Prieto JL et al (2010) Dielectrophoretic separation of heterogeneous stem cell populations. In: 14th international conference on miniaturized systems for chemistry and life sciences (MicroTAS 2010), The Netherlands
Pysher MD, Hayes MA (2007) Electrophoretic and dielectrophoretic field gradient technique for separating bioparticles. Anal Chem 79(12):4552–4557
Sackmann EK, Fulton AL, Beebe DJJN (2014) The present and future role of microfluidics in biomedical research. Nature 507(7491):181
Sano MB et al (2011) Contactless dielectrophoretic spectroscopy: examination of the dielectric properties of cells found in blood. Electrophoresis 32(22):3164–3171
Shafiee H et al (2010) Selective isolation of live/dead cells using contactless dielectrophoresis (cDEP). Lab Chip 10(4):438–445
Shapiro HM (2005) Practical flow cytometry. Wiley, New York
So J-H, Dickey MD (2011) Inherently aligned microfluidic electrodes composed of liquid metal. Lab Chip 11(5):905–911
Song H et al (2008) Continuous-mode dielectrophoretic gating for highly efficient separation of analytes in surface micromachined microfluidic devices. J Micromech Microeng 18(12):125013
Song H et al (2015) Continuous-flow sorting of stem cells and differentiation products based on dielectrophoresis. Lab Chip 15(5):1320–1328
Sun M et al (2016) Continuous on-chip cell separation based on conductivity-induced dielectrophoresis with 3D self-assembled ionic liquid electrodes. Anal Chem 88(16):8264–8271
Tang SY et al (2015) Creation of liquid metal 3D microstructures using dielectrophoresis. Adv Func Mater 25(28):4445–4452
Voldman J (2006) Electrical forces for microscale cell manipulation. J Annu Rev Biomed Eng 8:425–454
Voldman J et al (2002) A microfabrication-based dynamic array cytometer. Anal Chem 74(16):3984–3990
Wang Z, Zhe J (2011) Recent advances in particle and droplet manipulation for lab-on-a-chip devices based on surface acoustic waves. Lab Chip 11(7):1280–1285
Wognum AW, Eaves AC, Thomas TE (2003) Identification and isolation of hematopoietic stem cells. Arch Med Res 34(6):461–475
Wu Y et al (2017) Fluid pumping and cells separation by DC-biased traveling wave electroosmosis and dielectrophoresis. Microfluid Nanofluid 21(3):38
Yang J et al (1999) Cell separation on microfabricated electrodes using dielectrophoretic/gravitational field-flow fractionation. Anal Chem 71(5):911–918
Yoon YK et al (2003) Integrated vertical screen microfilter system using inclined SU-8 structures. In: The sixteenth annual international conference on micro electro mechanical systems. MEMS-03 Kyoto. IEEE. 2003. IEEE
Zhang C et al (2010) Dielectrophoresis for manipulation of micro/nano particles in microfluidic systems. Anal Bioanal Chem 396(1):401–420
Zhang J et al (2016) Fundamentals and applications of inertial microfluidics: a review. Lab Chip 16(1):10–34
Zhao K et al. (2019) Continuous cell characterization and separation by microfluidic AC dielectrophoresis. Anal Chem
Zhao K, Li D (2018) Tunable droplet manipulation and characterization by AC-DEP. ACS Appl Mater Interfaces 10(42):36572–36581
Zhao K, Li DJS, Chemical AB (2017) Continuous separation of nanoparticles by type via localized DC-dielectrophoresis using asymmetric nano-orifice in pressure-driven flow. Sens Actuators B Chem 250:274–284

Publisher's Note Springer Nature remains neutral with regard to jurisdictional claims in published maps and institutional affiliations.